

Assessment of shear strength of existing prestressed concrete bridge beams: Full-scale tests and numerical simulations

Prof. Eng. A. Lupoi
Sapienza University of Rome

Eng. A. Ficociello
Studio Speri Società di Ingegneria S. r. l.

Eng. M. Malavisi
Movyon

ABSTRACT: The obsolescence and the end of service lifetime of a big portion of our infrastructure, culminated with recent catastrophic bridge collapses, determine an increasing need to implement monitoring activities and safety assessment of existing bridges and viaducts. As stated in numerous studies and experimental evidence, shear strength is one of the critical issues concerning existing bridges. In order to deepen the knowledge on structural shear behavior, an experimental campaign on full-scale prestressed concrete girders sampled from an existing structure has been performed in the structures laboratory of the University of Pavia (Italy). This study illustrates the results of experimental tests and numerical finite element simulations, which have been performed both to obtain a comparison with experimental data and to study the main contributing factors to the collapse of the girder for shear type failure. The failure strength obtained from experimental testing has been compared with the shear strength calculated according to different strength models presented both in design codes and in the literature; therefore the accuracy of such models will be assessed in order to define the most suitable approach to assess girder shear strength. Translated with www.DeepL.com/Translator (free version)

1 INTRODUCTION

Since the Second World War, many bridges and viaducts have been built, most of which, still in use, are gradually reaching the end of their service life; for these reasons assessment of existing bridges is becoming more important for retrofit planning.

In order to carry out an assessment, bridge beams may present deficits related to their load-bearing capacity. Numerous studies and experimental tests have shown that lack of shear strength is one of the main typical issues characterizing these structures.

As already pointed out by several authors [6], nowadays there are several factors leading to low levels of safety against shear stress; since the 1950s, there has been a significant increase in the number of commercial vehicles, as well as the load carried by the trucks has increased over time. This trend is reflected in traffic load models of current code-law, the current load model proposed by Italian [2] and European technical standards [1] prescribe indeed the use of higher shear actions than the one previously used and presented within older versions.

Provisions given within past versions of design codes for design and assessment against shear actions have been revised several times since construction of our infrastructure bridges and viaducts. While in the past shear assessment was based on checking principal tensile stresses at non-cracked stage, it is now performed using methods based on the theory of tension fields or approaches developing truss models (truss with variable inclination) that refer to an ultimate limit state collapse scenario. In general, girders designed using a method that relies solely on the control of principal tensile stress contain a low amount of transverse reinforcement, given that no minimum amount of shear reinforcement was specified in the design codes of the time.

To study the behavior of existing bridge girders, load tests up to failure were performed on three prestressed concrete beams removed from the deck of a bridge; in addition dynamic identification tests were performed during loading history. Finally, the results of numerical simulations and strength models available in the literature allowed the validation of the experimental results.

2 EXPERIMENTAL CAMPAIGN

2.1 Specimen properties

The three specimens consist in a precast double “T” girders (type TAS 120/46), with an height of 1200mm and a width of 460mm. The beams, with a span length of $L=24.30$ m, are prestressed using 34Ø3/8” pre-tensioned strands (52mm² cross-section) and one 12Ø7 mm post-tensioned tendon (462mm² cross-section). The longitudinal rebar consists of 6Ø8 located at both top and bottom girder flanges; Table 1 shows the amount of transversal reinforcement in the beam, assuming as abscissa $x=0$ mm the section of extremity of the beam.

Table 1. Shear reinforcement.

Position	Spacing	Diameter	Legs
	mm	mm	-
$0\text{mm} \leq x < 180\text{mm}$	50	10	2
$180\text{mm} \leq x < 580\text{mm}$	100	10	2
$580\text{mm} \leq x < 6520\text{mm}$	180	10	2
$6520\text{mm} \leq x < L/2$	270	10	2

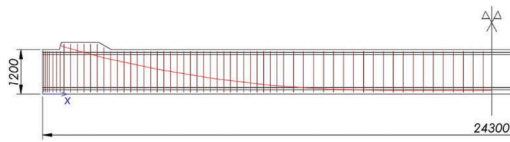


Figure 1. Longitudinal profile.

Investigations and tests were carried out on site to determine material properties; compressive strength resulting from destructive tests was corrected taking into account the geometry of the specimen and the disturbance caused to the same, obtaining an average crushing strength equal to $f_{cm}=46,3\text{MPa}$ and an elastic modulus of $E_c=34'841\text{MPa}$. There is no information of maximum aggregates size; however, from visual observations, the maximum diameter of the aggregates appears to be no more than 25mm.

Direct tensile tests resulted on an average yield strength $f_{ym}=347\text{MPa}$ and an ultimate tensile strength $f_{tm}=539\text{MPa}$, with elastic modulus $E_s=210'000\text{MPa}$.

The prestressing reinforcement consists of pre-tensioned strands with $f_{pt} \geq 1800\text{MPa}$ and a post-tensioned tendon with strength $f_{ps} \geq 1650\text{MPa}$.

The prestressing stress was evaluated performing tension release tests on the concrete at bottom flange of the beam.

In addition to the pre-existing state of deterioration of the beams (the reason for their removal from the deck), further damage was caused to the

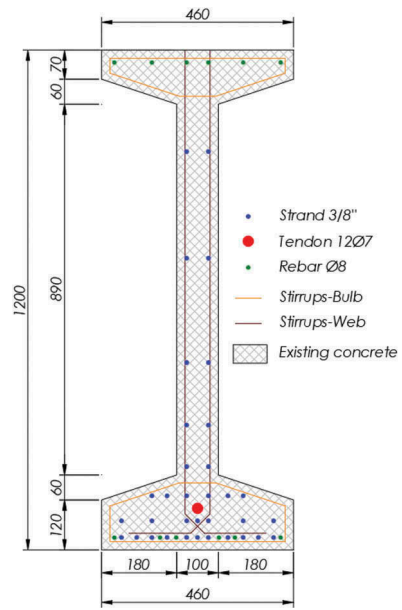


Figure 2. Geometry and reinforcement of the beam (mid-span section).

specimens during stripping operations; in particular, with the removal of the slab, the anchoring blocks of the post-tensioned tendon and some portions of the girder top were damaged. The resisting cross section of the girders was further weakened at the time of deconstruction at the connection to the bracing concrete beam, due to both the voids allowing reinforcement to pass through girder web and the damages occurred to the top of the girders.

2.2 Test setup

To study the behavior of the beams, four-point load tests and dynamic characterization tests were performed. In order to ensure a simple support static scheme, the beam was placed on cylindrical joints positioned at about 0.54 m from the end of the beam, with girders spanning over a length of 23.22 m. The trestles were positioned to apply punctual loads at about 3.15 m from both ends of the beam as shown in Figure 3.

Thirty-two linear displacement transducers were placed on the beam to evaluate girder displacements and rotations. A particular scrutiny was put on transducers located on the web at a section in between the bearings and load application points to obtain local deformations due to shear forces. At each load step (beginning of test and downstream of each cyclic load), a sequence of mechanical impact was performed on each specimen in order to identify its dynamic response in the Y and Z directions.

Three accelerometers and three geophones were installed on the specimen, paired and arranged at $1/4$, $1/2$, and $3/4$ of the girder span, respectively.

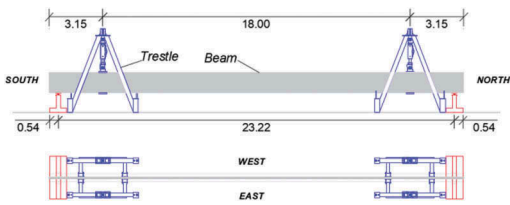


Figure 3. Test setup.

Each specimen was subjected to an out-of-plane action applied to the beam web at both centerline and $\frac{1}{4}$ length, and also impacts in the vertical direction.

Cyclic load tests were performed with progressive increase of the load after each cycle until the failure of the specimen. All the tests were run under force control, imposing on the two actuators the achievement of the target force value in a determined time, depending on the adopted speed, 1 or 2 kN/s. Figures 4-5-6 shows the loading history associated to the three tests performed.

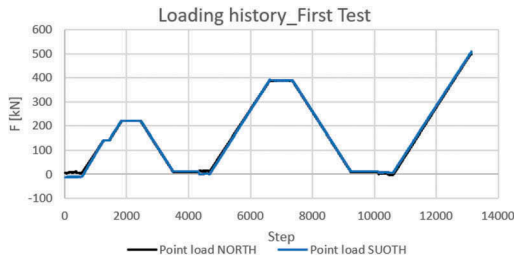


Figure 4. Loading history-First Test.

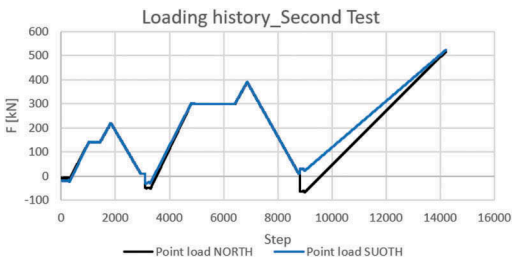


Figure 5. Loading history-Second Test.

2.3 Test results

Results of the load tests were expressed in such a way as to associate the corresponding value of the force applied with the measured quantity (vertical displacements, displacements of the supports, web

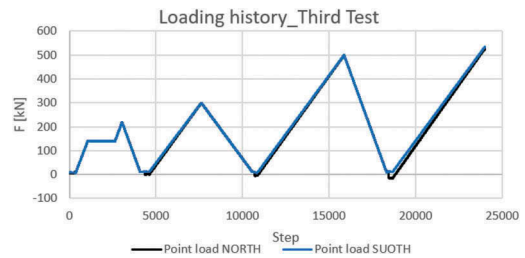


Figure 6. Loading history-Third Test.

deformations). Figures 7-8-9 shows the force-displacement diagrams at point load.

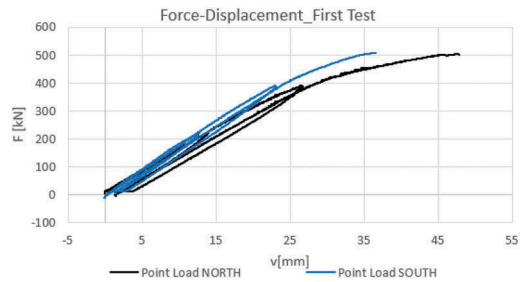


Figure 7. Force-Displacement at point load-First Test.

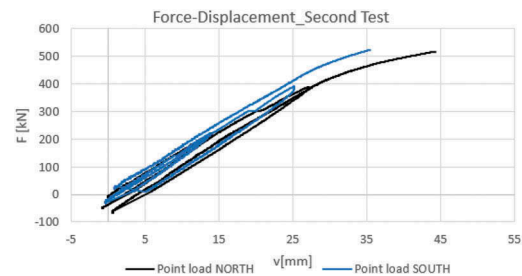


Figure 8. Force-Displacement at point load -Second Test.

The failure occurred from the north side of the beam. For all three tests, the experimental curves associated with the NORTH actuator show larger displacements due to greater deformability of the NORTH support system.

Table 2 shows the average load F applied and the shear V and bending M force at failure section.

During the first load test, the beam broke at the main beam-cross beam intersection, a vulnerable section due to the absence of a portion of the upper flange and the through holes in the web. Given the first test outcomes, the upper flange was reinforced in order to restore the section for the subsequent load tests. During the second and third tests, the failure of the

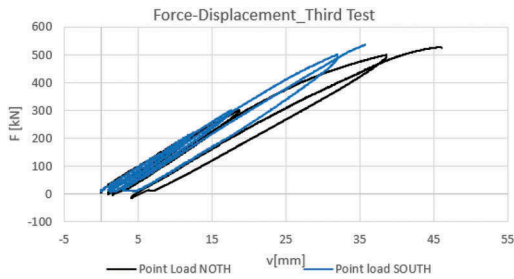


Figure 9. Force-Displacement at point load -Third Test.

Table 2. Applied load, shear and bending force at failure point.

Prova	F	V	M
	kN	kN	kNm
First Test	505	503	1300
Second Test	513	514	1345
Third Test	531	529	1381

beam occurred, as expected, in a zone between the support and the point of application of the force (Figure 13). Once the principal tensile stress in the web was exceeded, the initiation and propagation of the first shear cracks occurred immediately after, so the failure of the compressed portion of the top flange occurred: this type of failure has been identified as *shear-compression failure*.

The collapse of the beam could also be attributable to the failure of the section by bending with crush of the compression zone; in fact, without the collaborating slab, high compressive stresses are generated on the upper bulb of the beam (*flexural-compression failure*).



Figure 10. Beam failure-First Test.

Geophones and accelerometers recording signals during the application of the mechanical impulses, one in the Y direction and the other in the Z direction, allowed to identify the natural frequency



Figure 11. Beam failure-Second Test.



Figure 12. Beam failure-Third Test.

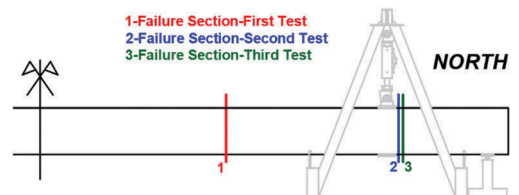


Figure 13. Failure section.

of vibration of the beam. After filtering the signal with a bandpass filter in a frequency range of 1-50 Hz to remove any electrical noise and bias, a spectral analysis was carried out using *Fast Fourier Transform (FFT)*. By obtaining the frequency spectra it was possible to identify the points of maximum amplitude that correspond to the frequency of the girders.

Tables 3-4-5 show the fundamental frequencies of vibration in the transverse direction (Y direction) at sections $x=L/4$ and $x=L/2$ and in the vertical direction (Z direction) at section $x=L/2$.

As shown on the results in Tables 3-4-5 the frequencies of the First Test in transverse direction at $x=L/4$ and Third Test in transverse direction at $x=L/4$ and $x=L/2$ can only show a decreasing trend

Table 3. First mode vibration frequency in transverse direction ($x=L/4$).

Direction Y	First Test	Second Test	Third Test
$x=L/4$	f [Hz]	f [Hz]	f [Hz]
Pre-test	2.18	2.87 3.02	
Post-test 1	2.13	3.03	2.96
Post-test 2	2.04	2.96	2.75
Post-test 3 -	-	2.48	

Table 4. First mode vibration frequency in transverse direction ($x=L/2$).

Direction Y	First Test	Second Test	Third Test
$x=L/2$	f [Hz]	f [Hz]	f [Hz]
Pre-test	2.13	2.87	3.01
Post-test 1	2.17	3.02	2.96
Post-test 2	2.04	2.96	2.75
Post-test 3 -	-	2.48	

Table 5. First mode vibration frequency in vertical direction ($x=L/2$).

Direction Z	First Test	Second Test	Third Test
$x=L/2$	f [Hz]	f [Hz]	f [Hz]
Pre-test	5.82	5.92	5.96
Post-test 1	9.63	6.69	5.82
Post-test 2	7.04	7.63	6.63
Post-test 3 -	-	6.40	

consistent with a progressive damage of the beam. The increase of frequency recorded during other loading steps can presumably be associated to post-tensioning of the cable during the test, resulting in an increase of beam stiffness. In the transverse direction the fundamental frequencies of vibration of the beam can be reasonably assumed in the range 2-3Hz while in the vertical direction 5.5-7.5Hz.

3 NUMERICAL SIMULATION

3.1 Finite element models

In order both to obtain a comparison with the experimental data and to study the determining factors to the behavior of the beam up to the collapse, numerical simulations have been performed, with finite element modeling (FEM) by linear and non-linear analyses.

The linear analysis (by means of finite element calculation software *SAP2000* [12]) was performed with the aim of evaluating the natural modes of vibration by means of modal analysis and to study, in detail, the tensional state and deformation of the beam, useful data for the validation of the results of the tension release tests.

The non-linear analysis was performed with the basic version of the *VecTor2* [11] computational code, with *FormWorks* [11] pre-processor and *Augustus* post-processor. The computational code, is well suited for the analysis of two-dimensional reinforced concrete structures and is based on the following theories:

1. *Modified Compression Field Theory* (Vecchio e Collins, 1986) [8];
2. *Disturbed Stress Field Model* (Vecchio, 2000) [9].

The models used for linear analyses provided, for a simply supported beam, consistent results with the test setup illustrated in Figure 3. The prestressing system consisting of both pre-tensioned strands and post-tensioned tendon was considered using *tendon* elements. The value of stresses obtained from tension release tests was assigned to each of those elements. The mechanical properties of the materials are as illustrated in §2.1.

For the realization of the plane model used for the nonlinear analysis, symmetry of loads and constraints allowed modeling of only half of the beam, enabling only vertical displacement of the middle section (symmetry section). Each portion of the beam was modeled assigning to the various parts of the element the thicknesses shown in Figure 2. Stirrups and longitudinal reinforcement, consisting of pre-stressed tendons and rebars, were considered as smeared reinforcement in the various parts of the structural element; the post-tensioned tendon was instead considered as a truss element. In order to obtain results in agreement with the experimental ones, the numerical model has included the defects observed on the tested beams, and:

1. in the sections between the support and the point of application of the load, due to the presence of some portions of the top flange not restored, the wings of top flange were not considered cooperating;
2. the incomplete effectiveness of the reinforcement of the top flange in the central area of the beam has been considered, reducing the width of top flange by 15% (from 460mm to 400mm); this assumption is also justified by the fact that the action of self weight and prestressing, generates effects only in the original section, while the restored top flange becomes collaborating only in response to external loads;
3. the section of the transversal reinforcement consisting of stirrups has been reduced by 15% (from Ø10 to Ø9,22) due to the presence of oxidation/corrosion;

- on the post-tensioned cable, after the failure of the beam, it was possible to observe the state of degradation with corrosion of the cable and absence of grout; therefore a reduction of the cable section of 15% (from 12Ø7 to 12Ø6,45) and a further reduction of the prestressing action was considered, bringing the losses of tension from 22% (as designed) to 30% (from 900MPa to 800MPa);
- in some sections of the beam it has been observed the breakage and/or corrosion of most of the pre-tensioned cables present in the first reinforcement level of the bottom flange; however, given their nature, the pre-tensioned cables remain cooperating with the section in the non-damaged areas and therefore it has been considered an equivalent deterioration in the first reinforcement level at the rate of 4 broken cables.

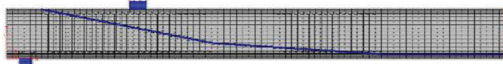


Figure 14. FEM model for non-linear analysis.

The loading history is cyclic and includes two intermediate loading steps before reaching the failure. A view of the FEM model is shown in Figure 14.

3.2 Linear analysis results

Beam vibration frequencies and strains state were determined using linear analysis and the results are summarized in Table 6.

As presented in the table above, the frequency of the first mode of vibration in transverse direction

Table 6. Frequency and period of vibration in transverse direction Y and vertical direction Z.

Mode	Frequency Y	Period Y	Frequency Z	Period Z
	f [Hz]	T [s]	f [Hz]	T [s]
First	4.413	0.227	4.688	0.213
Second	12.356	0.081	17.820	0.056
Third	24.399	0.041	33.777	0.030

Y (4.413Hz) is higher than the one obtained experimentally before the start of the tests (~3Hz); this is due to the presence of perfect constraints modelled in the simplified model used for the linear analysis while, actually, the transverse restraints have a finite stiffness depending on the stiffness properties of the steel stands. In the vertical Z direction, the frequency of the first mode (4.688 Hz) is lower than the experimentally recorded frequencies (~6Hz); in this case, the presence

of perfect constraints (no friction) and the absence of actuators in the linear model lead to a system with a lower degree of constraint with lower vibration frequencies.

The model realized with *brick* elements, where the beam is only subjected to the self-weight and the action of the prestressing system, has allowed to determine the initial deformation state of the beam. The strain recorded in the middle section at the side face of the lower bulb is 453µε (Figure 15); this value is close to the one obtained from tension release tests, varying between 406-436µε.

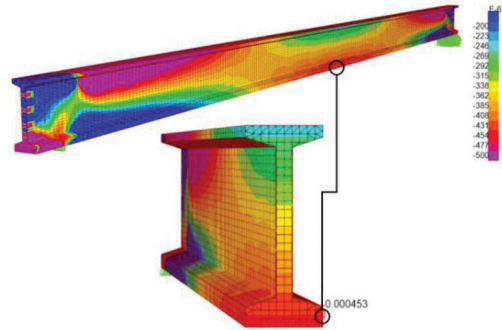


Figure 15. Deformation state of the beam subjected to self-weight and prestressing action.

3.3 Non-linear analysis results

Non-linear analysis allowed to simulate accurately the behavior of the beam till its failure. For the numerical simulation, a load history with cyclic load in force control was considered, similarly to loading cycles applied experimentally; in particular, the first load cycle aims at reaching the decompression of the beam by reaching a load of 225kN, while the second load cycle involves reaching a load of 450kN, with exceeding the principal tensile stress on the web and starting the excursion in the plastic field. The load history used for the numerical simulation is shown in Figure 16.

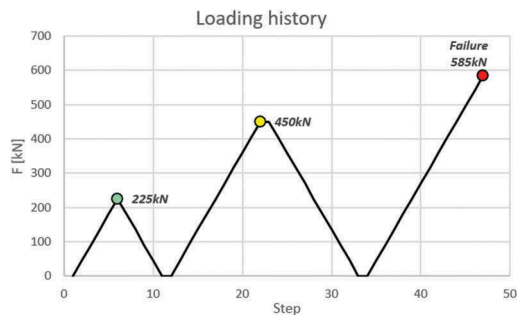


Figure 16. Loading history.

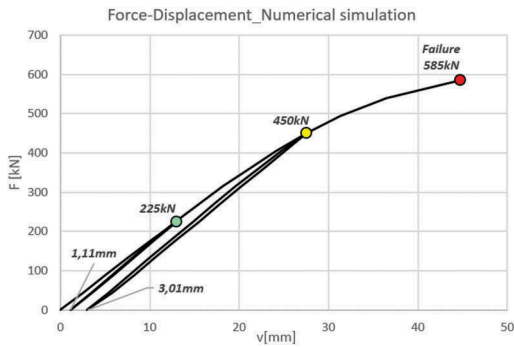


Figure 17. Force-displacement curve-numerical simulation.

Figure 17 Shows the Force-Displacement curve (read at the actuator) of the beam under the action of the load history previously illustrated.

Table 7 shows the load applied by the actuator F and the shear V and bending stress M at the first crack and at failure in correspondence of the failing section.

Table 7. Load and stress at first cracking and at failure.

Events	F	V	M
	kN	kN	kNm
First crack	495	441	1287
Failure	585	552	1521

Figures 18-19-20 provide the comparison between the force-displacement curve obtained from numerical simulations and the experimental tests.

As shown in Figures 18-19-20, the force-displacement curve obtained from non-linear analysis is close to the experimental response recorded at the SOUTH actuator; in the case of First Test, there is a greater discordance with the plastic field

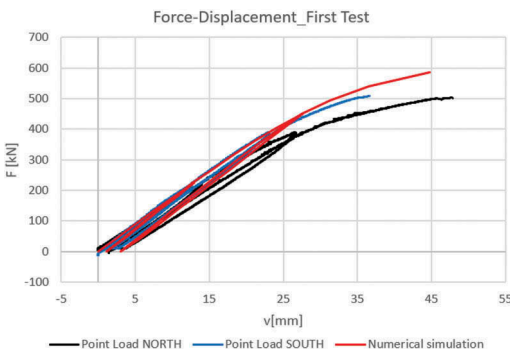


Figure 18. Comparison between numerical simulation curve and experimental curve-First Test.

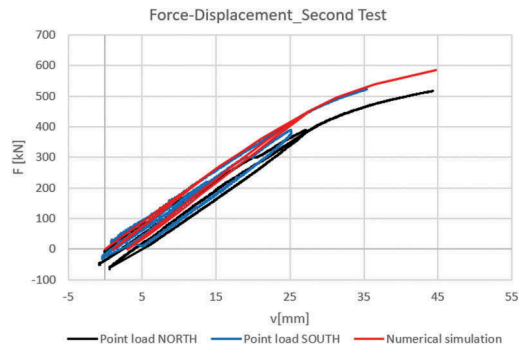


Figure 19. Comparison between numerical simulation curve and experimental curve-Second Test.

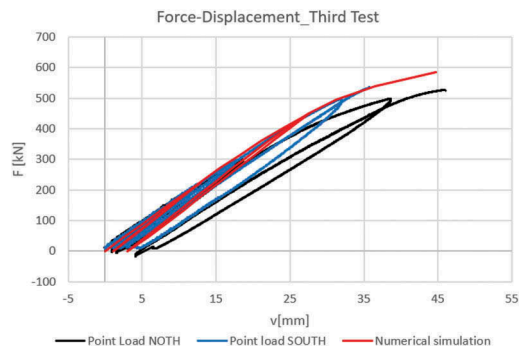


Figure 20. Comparison between numerical simulation curve and experimental curve-Third Test.

entry due to the failure that occurred in the central zone of the beam.

Figure 21 Shows the crack pattern at failure, corresponding with the peak of the force-strain curve.

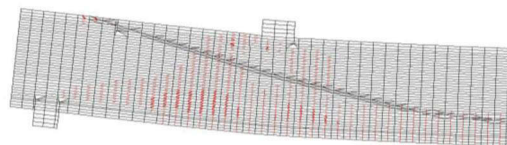


Figure 21. Crack pattern at failure.

In the failure configuration, the maximum width of the diagonal cracks on the web is less than 0.2mm; this value is in agreement with the absence of evident cracks on the web of the tested beams, with potential closure of the same upon removal of the applied load.

Figures 22-23-24 show compressive stress to compressive strength ratio σ_c/f_c , stress in stirrups σ_s , and crack inclination θ at failure, respectively.

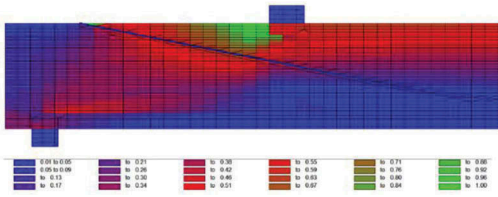


Figure 22. Ratio between compressive stress and compressive strength σ_c/f_c .

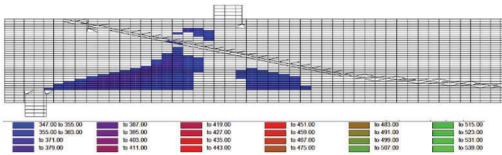


Figure 23. Tension in stirrups σ_s [MPa].

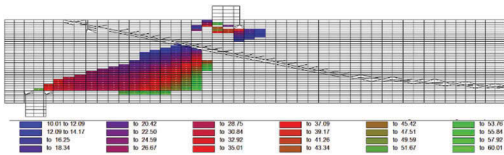


Figure 24. Inclination of diagonal crack θ [°].

Peak force is reached when the compressive stress close to the point of application of the force in the upper bulb reaches concrete compressive strength (area highlighted in green with $\sigma_c/f_c=1$ in Figure 22). This type of failure is anticipated by the activation of a shear resistant mechanism; before failure, in fact, the yield strength of stirrups is reached that consequently triggers a truss mechanism with an average inclination of the struts $\theta=29^\circ$ (from the experimental results θ ranges between 25° and 28°).

Figure 26 Shows the global response of the beam with a comparison between the bending moment

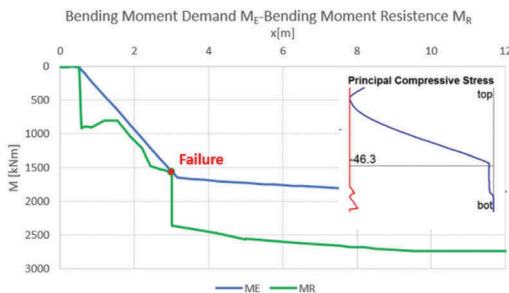


Figure 25. Comparison between bending moment demand ME and bending moment resistance.

demand M_E and bending moment resistance M_R . For the section failure is also reported the diagram of the principal compression stress in which it shows the achievement of compressive strength $f_{cm}=46,3\text{MPa}$.

The evolution of the behaviour of the beam up to failure and the absence of evident shear cracks, make the hypothesis of flexural-compression failure more plausible than a shear-compression failure. The beam, immediately after losing stiffness due to concrete crushing, is affected by a failure kinematic mechanism with a sub-vertical crack with progressive sliding and relative rotation between the left and the right portions. The type of kinematic mechanism just explained is validated from what observed during the experimental campaign during the second and third loading tests.

4 BEAM STRENGTH

4.1 Shear strength

For the evaluation of the shear strength, in addition to the experimental and nonlinear analysis results, a few models from the literature are presented. Those models describe both the behavior at the time of the first crack and at the collapse after the activation of a resistant mechanism that also involves the transverse reinforcement (Table 8).

The first-crack strength, evaluated with the formulation from Huber et al.[6] valid for the Uncracked Zone is close but lower than the first-crack resistance obtained by numerical simulation. The shear failure predictive models provide similar

Table 8. Shear strength V_R .

	V_R	Model
Strength	kN	-
First Crack	441	Numerical simulation
First Crack	425	Huber et al.-UN zone-[6]
Failure	503	Experimental-First Test
Failure	514	Experimental-Second Test
Failure	529	Experimental -Third Test
Failure	552	Numerical simulation
Failure	557	EC2 [1]/NTC18 [2]
Failure	588	Fib Model Code [3]
Failure	596	Cladera & Mari [4]
Failure	524	Herbrand [5]

results in terms of strength values as already illustrated by Huber et al.[7]; in fact, for an amount of reinforcement $\rho_w f_{yw} > 2\text{MPa}$, the strength models tend to provide similar strength values close to the failure load, without significant underestimation of the shear strength. For the considered beams value of $\rho_w f_{yw}$ is 3MPa, which falls into the scenario

previously described. Since most of the truss mechanism models are based on the static theorem application of limit analysis possibly refined to not provide overly cautious results, they should in most cases provide a shear capacity within a safety bound, not greater than the one obtained experimentally. Excluding Herbrand's model [5], other models in the literature have provided in the present study resistance values higher than the experimental data; this may be due to a non-perfect development of the classical resistant truss mechanism, in favor of a failure mechanism with early crushing of the compressed top bulb of the beam.

5 CONCLUSIONS

In this work, the results of an experimental and numerical campaign on prestressed concrete reinforced girders, claimed from an existing bridge, with a prestressing system consisting of pre-tensioned strands and a post-tensioned cable, are presented. Three beams simply supported over a span $L=24.30\text{m}$ were tested on four points with loads applied at a distance $a=2.6\text{m}$ from the supports. Comparing experimental results, numerical simulation outcomes and shear strength models in the literature, the following conclusions are drawn:

1. for prestressed beams with reinforcement quantity $\rho_w f_{yw} > 2\text{MPa}$ (typically found on beams with web thickness less than 200mm whose resistant section can be further reduced by the presence of post-tensioned cables), shear resistance models, including the simplest ones proposed by Italian [2] and European technical standards [1] but excluding Herbrand's model [5], have provided in the present study resistance values higher than the experimental data; the presence of geometrical defects or irregularity (for instance due to the absence of a portion of the slab and the crushing of the girder top in some sections) in conjunction with other common defects found on reinforced concrete bridge beams (corrosion of the stirrups, of the cables and further prestressing losses), may lead to a change of the usual shear resistance mechanism, in favor of other failure mechanisms such as flexural-compression failure. As a consequence shear resistance models presented in the literature cannot predict accurately shear strength or failure mode.

2. if any of the circumstances presented within the previous points occurs, it is necessary to refer to more refined shear strength models, or preferably to numerical simulations capable of identifying also other failure mechanisms

ACKNOWLEDGEMENT

Our special thanks to Autostrade per l'Italia S.p.a., Movyon and Eucentre to Eng. F. Germagnoli and Eng. F. Dacarro.

REFERENCES

1. EN 1992-1-1-Eurocode 2: Design of concrete structures - Part 1-1: General rules and rules for buildings.
2. Ministero delle Infrastrutture e dei trasporti, Decreto 17 gennaio 2018, Aggiornamento delle «Norme tecniche per le costruzioni». Italian Ministry of Infrastructures and Transportation; 2018 [in Italian].
3. Model Code 2010 - Final draft, Volume 2. (fib bulletin; No. 66). Fédération internationale du béton (fib). <http://www.fib-international.org/model-code-2010-final-draft-volume-2>.
4. Cladera A., Mari, A. (2004). Shear design procedure for reinforced normal and high-strength concrete beams using artificial neural networks. Part II: Beams with stirrups. *Engineering Structures*. 26. 927–936.
5. Herbrand M. (2017). Shear strength models for re-inforced and prestressed concrete members. 10.18154/RWTH-2017-06170.
6. Huber P., Vill M., Schweighofer A., Kollegger J. (2018). Full-scale shear tests on post-tensioned bridge girders of existing bridges. *Structural Concrete*. 19. 5–15.
7. Huber, Patrick & Huber, Tobias & Kollegger, Johann. (2016). Shear behavior of post-tensioned concrete beams with a low amount of transverse reinforcement.
8. F.J. Vecchio, M.P. Collins (1986). The modified compression-field theory for reinforced concrete elements subjected to shear. *ACI Journals*.
9. Vecchio, F. (2000). Disturbed Stress Field Model for Reinforced Concrete: Formulation *Journal of Structural Engineering-asce* 126. 10.1061/(ASCE)0733-9445(2000)126:9(1070).
10. Eucentre. Report Tecnico EUC201_2020E. Prove su travi in cap rimosse dal sottovia Santhià.
11. Wong P.S., Vecchio F.J., Trommels H. (2013). *Vector2 & Formworks user's manual-Second Edition*.
12. CSI, "SAP2000 Integrated Software for Structural Analysis and Design," Computers and Structures Inc., Berkeley, California.